Capacity and Coverage Optimization of Cellular Network Deployments for UAV Corridors

Saeed Karimi-Bidhendi[⋆], Giovanni Geraci[♯♭], and Hamid Jafarkhani[⋆]

[⋆]*Center for Pervasive Communications and Computing, Univ. of California, Irvine CA, USA*
[♯]*Telefónica Scientific Research and* [♭]*Universitat Pompeu Fabra (UPF), Barcelona, Spain*

***Abstract*—We introduce a novel mathematical framework for optimizing cellular network deployments, providing robust coverage and capacity for heterogeneous 3D user distributions. We establish necessary conditions and propose an iterative algorithm to fine-tune critical base station (BS) parameters, including location, horizontal bearing, vertical antenna tilt, and transmit power. In our case study, we optimize both existing and newly deployed BSs to support ground users and uncrewed aerial vehicles (UAVs) along designated corridors. Results indicate that the framework significantly enhances UAV connectivity while preserving near-optimal performance for ground users.**

I. Introduction

Robust air-to-ground connectivity is crucial for applications like drone delivery services, low-level aircraft operations, and advanced urban air mobility. Achieving 3D connectivity may require re-engineering the cellular network, which is currently optimized for 2D ground-level connectivity [1]–[3]. With flying users located within designated aerial paths or corridors, it becomes necessary to integrate them into the network and optimize coverage and capacity within these areas [4], [5].

The coverage and capacity of cellular networks depend heavily on base station (BS) deployment and antenna configuration. Optimizing these performance metrics is challenging due to interference coupling between cells, making the problem nonconvex and NP-hard [6]. Conflicting objectives further complicate this: maximizing coverage directs energy towards cell edges, while maximizing capacity favors cell-center users. Existing optimization methods, such as those from 3GPP, use stochastic simulations applied to small, homogeneous layouts [7], [8], but they do not generalize well to real-world networks. In practice, radio frequency planning tools rely on trial-and-error and field measurements, which are time-consuming and fail to provide scalable, near-optimal solutions.

These challenges are exacerbated with aerial users, e.g., uncrewed aerial vehicles (UAVs). Indeed, optimizing aerial coverage conflicts with legacy ground users, who benefit from downtilted cells [9]. Moreover, UAVs may perceive strong line-of-sight (LoS) interference from a plurality of cells [10]–[13]. Recent studies have addressed this through ad-hoc optimizations [14]–[17]. Advanced techniques like reinforcement learning (RL) and Bayesian optimization (BO) have also shown promise [18], [19]. RL adapts to dynamic environments but requires substantial data and has slow convergence, with potential for suboptimal configurations [6], [18]. BO offers faster, safer convergence, but struggles with computational complexity, limiting it to low-dimensional problems [19]. Despite these advancements, a scalable general mathematical framework for optimizing cellular networks for both ground users and UAV corridors is still lacking.

In this paper, we build on our previous work [20] to develop a comprehensive mathematical framework for cell deployment optimization, drawing inspiration from quantization theory [21]. This framework enables precise tuning of antenna parameters at each BS in a given deployment to achieve optimal coverage, capacity, or any desired trade-off. Additionally, it supports the optimization of new BS placements, including both site locations and antenna configurations. Our main contributions are as follows:

- We establish the necessary conditions and propose an iterative algorithm to optimize: (i) the vertical antenna tilts and transmit power at existing BSs, and (ii) the location, horizontal bearing, vertical tilt, and transmit power of newly deployed BSs, ensuring the best quality of service for a given geographical user distribution.
- We apply our framework to a practical cellular network to maximize capacity and coverage for both a heterogeneous distribution of ground users and 3D UAV corridors. The optimized configuration significantly enhances UAV performance with only a minor impact on ground user performance.

To the best of our knowledge, this is the first work to rigorously address these optimization goals while considering realistic network deployments, antenna radiation patterns, and propagation channel models.

II. System Model

The cellular network under consideration and the parameters to be optimized are depicted in Fig. 1 and outlined below.

A. Network Setup

1) Cellular Network: The structure of our network consists of N BSs that provide coverage and service to network users.

This work was supported in part by the NSF Award CNS-2229467, the Spanish State Research Agency through grants CNS2023-145384, PID2021-123999OB-I00, and CEX2021-001195-M, the UPF-Fractus Chair, and HORIZON-SESAR-2023-DES-ER-02 project ANTENNAE (101167288).

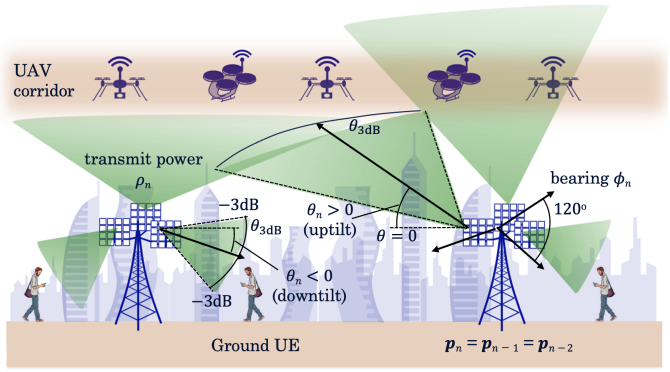

Fig. 1: Uptilted ($\theta_n > 0$) and downtilted ($\theta_n < 0$) BSs serving GUEs and UAV corridors, with θ_n, $\theta_{3\text{dB}}$, ϕ_n, and ρ_n denoting vertical tilt, vertical HPBW, horizontal bearing, and transmit power, respectively. Also, $\boldsymbol{p}_{n-2} = \boldsymbol{p}_{n-1} = \boldsymbol{p}_n$ denote the position of three co-located sectorized BSs.

The height, 2D location, and horizontal bearing of BS n is denoted by $h_{n,\text{B}}$, $\boldsymbol{p}_n \in \mathbb{R}^2$, and $\phi_n \in [-180°, 180°]$, respectively, for $n \in \{1, \cdots, N\}$. Additionally, for each n, the vertical antenna tilt and transmission power of BS n is denoted by $\theta_n \in [-90°, 90°]$ and $\rho_n \in (-\infty, \rho_{\max}]$, respectively, where $\rho_{\max}$ is the maximum BS transmit power in dBm.

Sectorized Cells: While our framework can accommodate arbitrary customization of BS deployment, here we focus on the common sectorized cells, with each deployment site consisting of three BSs positioned at the same location and with equally spaced horizontal bearings, i.e.:

$$\widehat{\boldsymbol{p}}_m = \boldsymbol{p}_{n-2} = \boldsymbol{p}_{n-1} = \boldsymbol{p}_n, \tag{1}$$

$$\widehat{\phi}_m = \phi_{n-2} = \phi_{n-1} - 120° = \phi_n - 240°, \tag{2}$$

where $\widehat{\boldsymbol{p}}_m$ and $\widehat{\phi}_m$ are the location and the reference bearing of site $m = \frac{n}{3}$, respectively. Let $\boldsymbol{\Theta} = (\theta_1, \cdots, \theta_N)$, $\boldsymbol{\rho} = (\rho_1, \cdots, \rho_N)$, $\widehat{\boldsymbol{P}} = (\widehat{\boldsymbol{p}}_1, \cdots, \widehat{\boldsymbol{p}}_{\frac{N}{3}})$, and $\widehat{\boldsymbol{\Phi}} = (\widehat{\phi}_1, \cdots, \widehat{\phi}_{\frac{N}{3}})$ denote the collection of BS tilts, powers, site locations, and reference bearings, respectively.

Existing vs. Newly Deployed BSs: While the locations and bearings of some BSs are fixed as part of the existing infrastructure, we optimally deploy and configure new BSs. We assume that there are $N - M$ BSs whose site locations and reference bearings are fixed a priori, denoted as $\underline{\widehat{\boldsymbol{P}}} = \left(\widehat{\boldsymbol{p}}_1, \cdots, \widehat{\boldsymbol{p}}_{\frac{N-M}{3}}\right)$ and $\underline{\widehat{\boldsymbol{\Phi}}} = \left(\widehat{\phi}_1, \cdots, \widehat{\phi}_{\frac{N-M}{3}}\right)$, respectively. In addition, there are M new BSs to be deployed onto $\frac{M}{3}$ new sites at locations $\overline{\widehat{\boldsymbol{P}}} = \left(\widehat{\boldsymbol{p}}_{\frac{N-M}{3}+1}, \cdots, \widehat{\boldsymbol{p}}_{\frac{N}{3}}\right)$ and with reference bearings $\overline{\widehat{\boldsymbol{\Phi}}} = \left(\widehat{\phi}_{\frac{N-M}{3}+1}, \cdots, \widehat{\phi}_{\frac{N}{3}}\right)$.

2) Ground Users and UAV Corridors: BSs serve two types of users: (i) Ground users (GUEs) distributed over a 2D region Q_{G} according to the density function $\lambda_{\text{G}}(\boldsymbol{q})$, with fixed height h_{G}; (ii) UAVs traversing the region $Q_{\text{U}} = \bigcup_{u=1}^{N_U} Q_u$ consisting of N_U aerial corridors, whose distribution over Q_{U} is denoted by $\lambda_{\text{U}}(\boldsymbol{q})$. Let $\lambda(\boldsymbol{q}) = r\lambda_{\text{G}}(\boldsymbol{q}) + (1-r)\lambda_{\text{U}}(\boldsymbol{q})$ be the users' distribution over the entire region $Q = Q_{\text{G}} \cup Q_{\text{U}}$, where $r \in [0, 1]$ is the mixture weight prioritizing the optimization for each network user type and controlling the corresponding trade-off.

Cell Partitioning: Each user is associated with the BS providing the largest received signal strength (RSS). Therefore, the region Q is partitioned into N disjoint regions $\boldsymbol{V} = (V_1, \cdots, V_N)$ such that network users in Region V_n are associated with BS n for each $n \in \{1, \cdots, N\}$.

3) Channel Model: We focus on long-term cell planning through optimal BS configuration to achieve the best coverage-capacity trade-offs. In practice, these design choices are driven by large-scale fading, since small-scale fading primarily affects instantaneous, narrowband signal quality and can be mitigated with channel coding. Therefore, in the following, we focus on modeling large-scale fading as done in 3GPP [7], [8].

Antenna Gain: BSs use directional antennas with vertical and horizontal half-power beamwidths of $\theta_{3\text{dB}}$ and $\phi_{3\text{dB}}$, respectively. The total antenna gain at user location $\boldsymbol{q}$ from BS n is given by $A_{n,\boldsymbol{q}} = A_{\max} + A^{\text{V}}_{n,\boldsymbol{q}} + A^{\text{H}}_{n,\boldsymbol{q}}$ in which [8]:

$$A^{\text{V}}_{n,\boldsymbol{q}} = -\frac{12}{\theta^2_{3\text{dB}}}\left[\theta_{n,\boldsymbol{q}} - \theta_n\right]^2, \quad A^{\text{H}}_{n,\boldsymbol{q}} = -\frac{12}{\phi^2_{3\text{dB}}}\left[\phi_{n,\boldsymbol{q}} - \phi_n\right]^2, \tag{3}$$

and $A_{\max}$ is the maximum antenna gain at the boresight. The elevation angle $\theta_{n,\boldsymbol{q}}$ and horizontal bearing $\phi_{n,\boldsymbol{q}}$ between user location $\boldsymbol{q}$ and BS n are expressed as follows:

$$\theta_{n,\boldsymbol{q}} = \tan^{-1}\left(\frac{q_{\text{z}} - p_{n,\text{z}}}{\sqrt{(q_{\text{x}} - p_{n,\text{x}})^2 + (q_{\text{y}} - p_{n,\text{y}})^2}}\right), \tag{4}$$

$$\phi_{n,\boldsymbol{q}} = \begin{cases} \tan^{-1}\left(\frac{q_{\text{y}} - p_{n,\text{y}}}{q_{\text{x}} - p_{n,\text{x}}}\right) + 180° \times 2c & \text{if } q_{\text{x}} - p_{n,\text{x}} > 0 \\ \tan^{-1}\left(\frac{q_{\text{y}} - p_{n,\text{y}}}{q_{\text{x}} - p_{n,\text{x}}}\right) + 180° \times (2c+1) & \text{if } q_{\text{x}} - p_{n,\text{x}} < 0, \end{cases}$$

with integer c chosen such that $-180° \le \phi_{n,\boldsymbol{q}} - \phi_n \le +180°$.

Pathloss: The pathloss between user location $\boldsymbol{q}$ and BS n, denoted as $L_{n,\boldsymbol{q}}$, depends on their distance and is given by:

$$L_{n,\boldsymbol{q}} = a_{\boldsymbol{q}} + b_{\boldsymbol{q}} \log_{10}\left(\|\boldsymbol{q} - \boldsymbol{p}_n\|\right). \tag{5}$$

The parameter $a_{\boldsymbol{q}}$ depends on the carrier frequency while $b_{\boldsymbol{q}}$ is a function of line-of-sight condition and the pathloss exponent, which in turn relates to the BS deployment configuration, terrain, and the user height.

RSS and SINR: The RSS, measured in dBm, from BS n experienced at user location $\boldsymbol{q}$ is given by:

$$\begin{aligned} \texttt{RSS}^{(\text{n})}_{\text{dBm}}(\boldsymbol{q}) = \rho_n + A_{n,\boldsymbol{q}} - L_{n,\boldsymbol{q}} = \rho_n + A_{\max} \\ - \frac{12}{\theta^2_{3\text{dB}}}\left[\theta_{n,\boldsymbol{q}} - \theta_n\right]^2 - \frac{12}{\phi^2_{3\text{dB}}}\left[\phi_{n,\boldsymbol{q}} - \phi_n\right]^2 \\ - a_{\boldsymbol{q}} - b_{\boldsymbol{q}} \log_{10}\left(\|\boldsymbol{q} - \boldsymbol{p}_n\|\right). \end{aligned} \tag{6}$$

The wideband signal-to-interference-plus-noise ratio (SINR) in dB is defined as follows:

$$\texttt{SINR}^{(\text{n})}_{\text{dB}}(\boldsymbol{q}) = 10 \log_{10} \frac{10^{\frac{1}{10}\texttt{RSS}^{(\text{n})}_{\text{dBm}}(\boldsymbol{q})}}{\sum_{j \neq n} 10^{\frac{1}{10}\texttt{RSS}^{(\text{j})}_{\text{dBm}}(\boldsymbol{q})} + \sigma^2}, \tag{7}$$

where σ^2 denotes the thermal noise variance in linear units.

B. Key Performance Indicators (KPIs)

To pursue a coverage-capacity trade-off, we define a KPI that combines sum-log-rate and coverage, as follows.

1) Log-rate: We employ this metric since it balances rate maximization with fairness, and it is commonly used for proportional fairness and load balancing in cellular systems. Given the user location $\boldsymbol{q}$ and BS n, the log-rate is:

$$\gamma'^{(n)}(\boldsymbol{q}) = \log_2\Big(\log_2\big(1+\mathsf{SINR}^{(\mathsf{n})}_{\mathsf{lin}}(\boldsymbol{q})\big)\Big). \tag{8}$$

2) Coverage: This metric aims to minimize outage among network users by penalizing SINR values below a certain threshold. Given the user location $\boldsymbol{q}$ and BS n, coverage is a binary variable defined as follows:

$$\gamma''^{(n)}(\boldsymbol{q}) = \mathbb{1}\big(\mathsf{SINR}^{(\mathsf{n})}_{\mathsf{dB}}(\boldsymbol{q}) \geq T\big), \tag{9}$$

with $\mathbb{1}(\cdot)$ denoting the indicator function. We employ the following differentiable approximation to (9):

$$\widetilde{\gamma}''^{(n)}(\boldsymbol{q}) = \frac{1}{1+e^{-\kappa\left[\mathsf{SINR}^{(\mathsf{n})}_{\mathsf{dB}}(\boldsymbol{q})-T\right]}}, \tag{10}$$

where the parameter κ controls the steepness of the sigmoid approximation to the indicator function.

Using parameter β to control the tradeoff between log-rate and coverage, the capacity-coverage KPI is defined as:

$$\gamma^{(n)}(\boldsymbol{q}) = \beta\gamma'^{(n)}(\boldsymbol{q}) + (1-\beta)\widetilde{\gamma}''^{(n)}(\boldsymbol{q}). \tag{11}$$

III. Mathematical Framework

The performance function under consideration relates to maximizing the aforementioned KPI over all network users:

$$\begin{aligned}&\max_{\substack{\boldsymbol{V},\boldsymbol{\Theta},\boldsymbol{\rho},\overline{\widehat{\boldsymbol{P}}},\overline{\widehat{\boldsymbol{\Phi}}}\\ \boldsymbol{\rho}\in\boldsymbol{\Lambda}}} \mathcal{P}_\gamma\big(\boldsymbol{V},\boldsymbol{\Theta},\boldsymbol{\rho},\overline{\widehat{\boldsymbol{P}}},\overline{\widehat{\boldsymbol{\Phi}}}\big)\\ =&\max_{\substack{\boldsymbol{V},\boldsymbol{\Theta},\boldsymbol{\rho},\overline{\widehat{\boldsymbol{P}}},\overline{\widehat{\boldsymbol{\Phi}}}\\ \boldsymbol{\rho}\in\boldsymbol{\Lambda}}} \sum_{n=1}^{N}\int_{V_n}\gamma^{(n)}\big(\boldsymbol{q};\boldsymbol{\Theta},\boldsymbol{\rho},\overline{\widehat{\boldsymbol{P}}},\overline{\widehat{\boldsymbol{\Phi}}}\big)\lambda(\boldsymbol{q})d\boldsymbol{q},\end{aligned} \tag{12}$$

where $\boldsymbol{\Lambda} = (-\infty, \rho_{\max}]^N$ is the feasible region for the vector of BS transmission powers $\boldsymbol{\rho}$. Variants of the Lloyd algorithm in quantization theory [21], [22] have been applied to solve NP-hard optimization problems similar to the one in (12). Inspired by these techniques, we propose an alternating optimization algorithm that iterates between the five parameters $\big(\boldsymbol{V},\boldsymbol{\Theta},\ \boldsymbol{\rho},\overline{\widehat{\boldsymbol{P}}},\overline{\widehat{\boldsymbol{\Phi}}}\big)$ and in each iteration, it optimizes one of the parameters while keeping the remaining four unchanged, in a round-robin fashion. Elements of this procedure are as follows.

A. Optimal Cell Partitioning

We first derive the cell partitioning $\boldsymbol{V}^*$ that maximizes the performance function $\mathcal{P}_\gamma$.

Lemma 1. *Let $f:\mathbb{R}^+\to\mathbb{R}$ be a continuous and non-decreasing function. For a given set of $(\boldsymbol{V},\boldsymbol{\Theta},\boldsymbol{\rho},\boldsymbol{P},\boldsymbol{\Phi})$, let:*

$$F\left(\boldsymbol{V},\boldsymbol{\Theta},\boldsymbol{\rho},\boldsymbol{P},\boldsymbol{\Phi}\right) = \sum_{n=1}^{N}\int_{V_n} f\big(\mathsf{SINR}^{(\mathsf{n})}_{\mathsf{dB}}(\boldsymbol{q})\big)\lambda(\boldsymbol{q})d\boldsymbol{q}. \tag{13}$$

Then, the optimal cell partitioning that maximizes F for a given set of $(\boldsymbol{\Theta},\boldsymbol{\rho},\boldsymbol{P},\boldsymbol{\Phi})$ is given by

$$V_n^* = \{\boldsymbol{q}\in Q \mid \mathsf{RSS}^{(\mathsf{n})}_{\mathsf{dBm}}(\boldsymbol{q}) \geq \mathsf{RSS}^{(\mathsf{k})}_{\mathsf{dBm}}(\boldsymbol{q}),\ \ \forall k\neq n\}, \tag{14}$$

for each $n\in\{1,\cdots,N\}$, where ties are broken arbitrarily.

Proof. Let $\boldsymbol{V}^* = \arg\max_{\boldsymbol{V}} F\left(\boldsymbol{V},\boldsymbol{\Theta},\boldsymbol{\rho},\boldsymbol{P},\boldsymbol{\Phi}\right)$ denote the cell partitioning that maximizes F. Then, we have:

$$\begin{aligned}V_n^* &= \{\boldsymbol{q}\mid f\big(\mathsf{SINR}^{(\mathsf{n})}_{\mathsf{dB}}(\boldsymbol{q})\big) \geq f\big(\mathsf{SINR}^{(\mathsf{k})}_{\mathsf{dB}}(\boldsymbol{q})\big),\quad \forall k\neq n\}\\ &= \{\boldsymbol{q}\mid \mathsf{SINR}^{(\mathsf{n})}_{\mathsf{dB}}(\boldsymbol{q}) \geq \mathsf{SINR}^{(\mathsf{k})}_{\mathsf{dB}}(\boldsymbol{q}),\quad \forall k\neq n\}\\ &= \{\boldsymbol{q}\mid \mathsf{RSS}^{(\mathsf{n})}_{\mathsf{dBm}}(\boldsymbol{q}) \geq \mathsf{RSS}^{(\mathsf{k})}_{\mathsf{dBm}}(\boldsymbol{q}),\quad \forall k\neq n\}.\end{aligned} \tag{15}$$

The last equality in (15) follows from the proof of Proposition 4 in [20] and concludes the proof. □

The following proposition is the direct result of Lemma 1.

Proposition 1. *For a given $\boldsymbol{\Theta}$, $\boldsymbol{\rho}$, $\overline{\widehat{\boldsymbol{P}}}$, and $\overline{\widehat{\boldsymbol{\Phi}}}$, the optimal cell partitioning $\boldsymbol{V}^*$ that maximizes the performance function $\mathcal{P}_\gamma$ is given by (14) for each $n\in\{1,\cdots,N\}$, where ties are broken arbitrarily.*

Proof. The proof of Proposition 1 follows from Lemma 1 and the fact that both functions $f\big(\mathsf{SINR}^{(\mathsf{n})}_{\mathsf{dB}}(\boldsymbol{q})\big) = \log\big(\log(1+\mathsf{SINR}^{(\mathsf{n})}_{\mathsf{lin}}(\boldsymbol{q}))\big)$ and $f\big(\mathsf{SINR}^{(\mathsf{n})}_{\mathsf{dB}}(\boldsymbol{q})\big) = \frac{1}{1+e^{-\kappa\left[\mathsf{SINR}^{(\mathsf{n})}_{\mathsf{dB}}(\boldsymbol{q})-T\right]}}$ are continuous and non-decreasing. □

B. Optimal BS Tilts, Power, Locations, and Bearings

We employ gradient ascent to iteratively refine $\boldsymbol{\Theta}$, $\overline{\widehat{\boldsymbol{P}}}$, and $\overline{\widehat{\boldsymbol{\Phi}}}$. For the power $\boldsymbol{\rho}$, we use projected gradient ascent to make sure that it remains within the feasible region $\boldsymbol{\Lambda}$.

For this purpose, we need to calculate the partial derivatives of $\mathcal{P}_\gamma$ w.r.t. each parameter. Each partial derivative is comprised of two terms: (i) the derivative of the integrand, and (ii) the integral over the boundaries of V_n and its neighboring regions. For any point $\boldsymbol{q}$ on the boundary of neighboring regions V_n and V_m, the normal outward vectors have opposite directions but the same magnitude since $\mathsf{RSS}^{(\mathsf{n})}_{\mathsf{dBm}}(\boldsymbol{q}) = \mathsf{RSS}^{(\mathsf{m})}_{\mathsf{dBm}}(\boldsymbol{q})$ according to Proposition 1. Therefore, the sum of elements in term (ii) is zero [23]. As for (i), following the chain rule of calculus, the first component for each partial derivative is given by Propositions 2−5 below.

Proposition 2. *The partial derivative of the performance function $\mathcal{P}_\gamma$ w.r.t. the BS vertical antenna tilt θ_n is given by:*

$$\begin{aligned}\frac{\partial}{\partial\theta_n}\mathcal{P}_\gamma = \sum_{m=1}^{N}\int_{V_m}\Bigg[&\frac{\beta\cdot\log_2(e)\cdot\log_2(e)\cdot\ln 10\cdot 0.1}{\log_2\left(1+\mathsf{SINR}^{(\mathsf{m})}_{\mathsf{lin}}(\boldsymbol{q})\right)}\times\\ &\frac{\mathsf{SINR}^{(\mathsf{m})}_{\mathsf{lin}}(\boldsymbol{q})}{1+\mathsf{SINR}^{(\mathsf{m})}_{\mathsf{lin}}(\boldsymbol{q})} + \kappa(1-\beta)\cdot\sigma\Big(\kappa\big[\mathsf{SINR}^{(\mathsf{m})}_{\mathsf{dB}}(\boldsymbol{q})-T\big]\Big)\\ &\times\Big[1-\sigma\Big(\kappa\big[\mathsf{SINR}^{(\mathsf{m})}_{\mathsf{dB}}(\boldsymbol{q})-T\big]\Big)\Big]\Bigg]\cdot\frac{\partial}{\partial\theta_n}\mathsf{SINR}^{(\mathsf{m})}_{\mathsf{dB}}(\boldsymbol{q})\lambda(\boldsymbol{q})d\boldsymbol{q},\end{aligned} \tag{16}$$

where

$$\frac{\partial \mathsf{SINR}^{(\mathsf{m})}_{\mathsf{dB}}(\boldsymbol{q})}{\partial \theta_n} = \begin{cases} \frac{24}{\theta^2_{\mathsf{3dB}}}(\theta_{n,\boldsymbol{q}} - \theta_n), & \text{if } m = n \\ -\frac{\frac{24}{\theta^2_{\mathsf{3dB}}} \cdot (\theta_{n,\boldsymbol{q}} - \theta_n) \cdot \mathsf{RSS}^{(\mathsf{n})}_{\mathsf{lin}}(\boldsymbol{q}) \cdot \mathsf{SINR}^{(\mathsf{m})}_{\mathsf{lin}}(\boldsymbol{q})}{\mathsf{RSS}^{(\mathsf{m})}_{\mathsf{lin}}(\boldsymbol{q})}, & \text{o.w.} \end{cases} \tag{17}$$

and $\sigma(x) = \frac{1}{1+e^{-x}}$ *is the sigmoid function.*

Proposition 3. *The partial derivative of the performance function* $\mathcal{P}_\gamma$ *w.r.t. the BS transmission power* ρ_n *is given by:*

$$\frac{\partial}{\partial \rho_n}\mathcal{P}_\gamma = \sum_{m=1}^{N} \int_{V_m} \Bigg[\frac{\beta \cdot \log_2(e) \cdot \log_2(e) \cdot \ln 10 \cdot 0.1}{\log_2\left(1 + \mathsf{SINR}^{(\mathsf{m})}_{\mathsf{lin}}(\boldsymbol{q})\right)} \times \frac{\mathsf{SINR}^{(\mathsf{m})}_{\mathsf{lin}}(\boldsymbol{q})}{1 + \mathsf{SINR}^{(\mathsf{m})}_{\mathsf{lin}}(\boldsymbol{q})} + \kappa(1-\beta) \cdot \sigma\Big(\kappa\big[\mathsf{SINR}^{(\mathsf{m})}_{\mathsf{dB}}(\boldsymbol{q}) - T\big]\Big) \times \Big[1 - \sigma\Big(\kappa\big[\mathsf{SINR}^{(\mathsf{m})}_{\mathsf{dB}}(\boldsymbol{q}) - T\big]\Big)\Big]\Bigg] \cdot \frac{\partial}{\partial \rho_n}\mathsf{SINR}^{(\mathsf{m})}_{\mathsf{dB}}(\boldsymbol{q})\lambda(\boldsymbol{q})d\boldsymbol{q}, \tag{18}$$

where

$$\frac{\partial \mathsf{SINR}^{(\mathsf{m})}_{\mathsf{dB}}(\boldsymbol{q})}{\partial \rho_n} = \begin{cases} 1, & \text{if } m = n \\ -\frac{\mathsf{RSS}^{(\mathsf{n})}_{\mathsf{lin}}(\boldsymbol{q}) \cdot \mathsf{SINR}^{(\mathsf{m})}_{\mathsf{lin}}(\boldsymbol{q})}{\mathsf{RSS}^{(\mathsf{m})}_{\mathsf{lin}}(\boldsymbol{q})}, & \text{o.w.} \end{cases} \tag{19}$$

and $\sigma(x) = \frac{1}{1+e^{-x}}$ *is the sigmoid function.*

Proposition 4. *The gradient of the performance function* $\mathcal{P}_\gamma$ *w.r.t. the* m*-th site location* $\widehat{\boldsymbol{p}}_m$ *is:*

$$\nabla_{\widehat{\boldsymbol{p}}_m}\mathcal{P}_\gamma = \sum_{n=1}^{N} \int_{V_n} \Bigg[\frac{\beta \cdot \log_2(e) \cdot \log_2(e) \cdot \ln 10 \cdot 0.1}{\log_2\left(1 + \mathsf{SINR}^{(\mathsf{n})}_{\mathsf{lin}}(\boldsymbol{q})\right)} \times \frac{\mathsf{SINR}^{(\mathsf{n})}_{\mathsf{lin}}(\boldsymbol{q})}{1 + \mathsf{SINR}^{(\mathsf{n})}_{\mathsf{lin}}(\boldsymbol{q})} + \kappa(1-\beta) \cdot \sigma\Big(\kappa\big[\mathsf{SINR}^{(\mathsf{n})}_{\mathsf{dB}}(\boldsymbol{q}) - T\big]\Big) \times \Big[1 - \sigma\Big(\kappa\big[\mathsf{SINR}^{(\mathsf{n})}_{\mathsf{dB}}(\boldsymbol{q}) - T\big]\Big)\Big]\Bigg] \cdot \nabla_{\widehat{\boldsymbol{p}}_m}\mathsf{SINR}^{(\mathsf{n})}_{\mathsf{dB}}(\boldsymbol{q})\lambda(\boldsymbol{q})d\boldsymbol{q}. \tag{20}$$

If $n \notin \{3m-2, 3m-1, 3m\}$*, the term* $\nabla_{\widehat{\boldsymbol{p}}_m}\mathsf{SINR}^{(\mathsf{n})}_{\mathsf{dB}}(\boldsymbol{q})$ *is:*

$$\nabla_{\widehat{\boldsymbol{p}}_m}\mathsf{SINR}^{(\mathsf{n})}_{\mathsf{dB}} = -\frac{\mathsf{SINR}^{(\mathsf{n})}_{\mathsf{lin}}}{\mathsf{RSS}^{(\mathsf{n})}_{\mathsf{lin}}} \times \Big[\mathsf{RSS}^{(\mathsf{3m-2})}_{\mathsf{lin}} \cdot \nabla_{\boldsymbol{p}_{3m-2}}\mathsf{RSS}^{(\mathsf{3m-2})}_{\mathsf{dBm}} + \mathsf{RSS}^{(\mathsf{3m-1})}_{\mathsf{lin}} \cdot \nabla_{\boldsymbol{p}_{3m-1}}\mathsf{RSS}^{(\mathsf{3m-1})}_{\mathsf{dBm}} + \mathsf{RSS}^{(\mathsf{3m})}_{\mathsf{lin}} \cdot \nabla_{\boldsymbol{p}_{3m}}\mathsf{RSS}^{(\mathsf{3m})}_{\mathsf{dBm}}\Big]. \tag{21}$$

However, if $n \in \{3m-2, 3m-1, 3m\}$*, we have:*

$$\nabla_{\widehat{\boldsymbol{p}}_m}\mathsf{SINR}^{(\mathsf{n})}_{\mathsf{dB}} = \nabla_{\boldsymbol{p}_n}\mathsf{RSS}^{(\mathsf{n})}_{\mathsf{dBm}} - \frac{\Big[\mathsf{RSS}^{(\mathsf{n}')}_{\mathsf{lin}} \cdot \nabla_{\boldsymbol{p}_{n'}}\mathsf{RSS}^{(\mathsf{n}')}_{\mathsf{dBm}} + \mathsf{RSS}^{(\mathsf{n}'')}_{\mathsf{lin}} \cdot \nabla_{\boldsymbol{p}_{n''}}\mathsf{RSS}^{(\mathsf{n}'')}_{\mathsf{dBm}}\Big]}{\Big[\sum_{j \neq n}\mathsf{RSS}^{(\mathsf{j})}_{\mathsf{lin}} + \sigma^2_{\mathsf{lin}}\Big]}, \tag{22}$$

where $\{n, n', n''\} = \{3m-2, 3m-1, 3m\}$*. For each* n*, the term* $\nabla_{\boldsymbol{p}_n}\mathsf{RSS}^{(\mathsf{n})}_{\mathsf{dBm}}$ *is given by:*

$$\nabla_{\boldsymbol{p}_n}\mathsf{RSS}^{(\mathsf{n})}_{\mathsf{dBm}}(\boldsymbol{q}; \theta_n, \rho_n, \boldsymbol{p}_n, \phi_n) = \frac{-24}{\theta^2_{\mathsf{3dB}}}(\theta_{n,\boldsymbol{q}} - \theta_n) \cdot \frac{(h_{n,B} - h_{\boldsymbol{q}}) \cdot (\boldsymbol{p}_n - \boldsymbol{q})}{\|\boldsymbol{p}_n - \boldsymbol{q}\|^3 + \|\boldsymbol{p}_n - \boldsymbol{q}\|(h_{n,B} - h_{\boldsymbol{q}})^2} - \frac{24}{\phi^2_{\mathsf{3dB}}}(\phi_{n,\boldsymbol{q}} - \phi_n) \cdot \left(\frac{q_y - p_{n,y}}{\|\boldsymbol{q} - \boldsymbol{p}_n\|^2}, \frac{p_{n,x} - q_x}{\|\boldsymbol{q} - \boldsymbol{p}_n\|^2}\right) - \frac{b_{\boldsymbol{q}} \log_{10}(e) \cdot (\boldsymbol{p}_n - \boldsymbol{q})}{\|\boldsymbol{q} - \boldsymbol{p}_n\|^2 + (h_{\boldsymbol{q}} - h_{n,B})^2}. \tag{23}$$

Proposition 5. *The partial derivative of the performance function* $\mathcal{P}_\gamma$ *w.r.t. the site* m*'s reference bearing* $\widehat{\phi}_m$ *is:*

$$\frac{\partial}{\partial \widehat{\phi}_m}\mathcal{P}_\gamma = \sum_{n=1}^{N} \int_{V_n} \Bigg[\frac{\beta \cdot \log_2(e) \cdot \log_2(e) \cdot \ln 10 \cdot 0.1}{\log_2\left(1 + \mathsf{SINR}^{(\mathsf{n})}_{\mathsf{lin}}(\boldsymbol{q})\right)} \times \frac{\mathsf{SINR}^{(\mathsf{n})}_{\mathsf{lin}}(\boldsymbol{q})}{1 + \mathsf{SINR}^{(\mathsf{n})}_{\mathsf{lin}}(\boldsymbol{q})} + \kappa(1-\beta) \cdot \sigma\Big(\kappa\big[\mathsf{SINR}^{(\mathsf{n})}_{\mathsf{dB}}(\boldsymbol{q}) - T\big]\Big) \times \Big[1 - \sigma\Big(\kappa\big[\mathsf{SINR}^{(\mathsf{n})}_{\mathsf{dB}}(\boldsymbol{q}) - T\big]\Big)\Big]\Bigg] \cdot \frac{\partial \mathsf{SINR}^{(\mathsf{n})}_{\mathsf{dB}}(\boldsymbol{q})}{\partial \widehat{\phi}_m}\lambda(\boldsymbol{q})d\boldsymbol{q}. \tag{24}$$

If $n \notin \{3m-2, 3m-1, 3m\}$*, the term* $\frac{\partial \mathsf{SINR}^{(\mathsf{n})}_{\mathsf{dB}}(\boldsymbol{q})}{\partial \widehat{\phi}_m}$ *is:*

$$\frac{\partial \mathsf{SINR}^{(\mathsf{n})}_{\mathsf{dB}}}{\partial \widehat{\phi}_m} = -\frac{\mathsf{SINR}^{(\mathsf{n})}_{\mathsf{lin}}}{\mathsf{RSS}^{(\mathsf{n})}_{\mathsf{lin}}} \cdot \frac{24}{\phi^2_{3dB}} \cdot \sum_{t=3m-2}^{3m} \mathsf{RSS}^{(\mathsf{t})}_{\mathsf{lin}} \cdot (\phi_{t,\boldsymbol{q}} - \phi_t)\,. \tag{25}$$

However, if $n \in \{3m-2, 3m-1, 3m\}$*, we have:*

$$\frac{\partial \mathsf{SINR}^{(\mathsf{n})}_{\mathsf{dB}}}{\partial \widehat{\phi}_m} = \frac{24}{\phi^2_{3dB}}\Bigg[(\phi_{n,\boldsymbol{q}} - \phi_n) - \frac{\mathsf{SINR}^{(\mathsf{n})}_{\mathsf{lin}}}{\mathsf{RSS}^{(\mathsf{n})}_{\mathsf{lin}}} \times \Big(\mathsf{RSS}^{(\mathsf{n}')}_{\mathsf{lin}} \cdot (\phi_{n',\boldsymbol{q}} - \phi_{n'}) + \mathsf{RSS}^{(\mathsf{n}'')}_{\mathsf{lin}} \cdot (\phi_{n'',\boldsymbol{q}} - \phi_{n''})\Big)\Bigg], \tag{26}$$

where $\{n, n', n''\} = \{3m-2, 3m-1, 3m\}$*.*

C. Coverage-Capacity Optimization Algorithm

Our algorithm uses Propositions 1–5 as follows.

Algorithm 1. *Coverage-capacity maximization starts with a random initialization of the parameters and iterates among the following five steps until the convergence criterion is met:*

- *Given* $\boldsymbol{\Theta}$*,* $\boldsymbol{\rho}$*,* $\widehat{\boldsymbol{P}}$*, and* $\widehat{\boldsymbol{\Phi}}$*, optimize the cell partitioning* $\boldsymbol{V}$ *by assigning each user* $\boldsymbol{q}$ *to the base station that provides the highest RSS value at that user location, as per (14);*
- *Given* $\boldsymbol{V}$*,* $\boldsymbol{\rho}$*,* $\widehat{\boldsymbol{P}}$*, and* $\widehat{\boldsymbol{\Phi}}$*, apply gradient ascent to optimize the vertical tilts* $\boldsymbol{\Theta}$ *using the partial derivatives in (16);*
- *Given* $\boldsymbol{V}$*,* $\boldsymbol{\Theta}$*,* $\widehat{\boldsymbol{P}}$*, and* $\widehat{\boldsymbol{\Phi}}$*, apply projected gradient ascent with the feasible region* $\boldsymbol{\Lambda}$ *to optimize the BS transmission powers* $\boldsymbol{\rho}$ *using the partial derivatives in (18);*
- *Given* $\boldsymbol{V}$*,* $\boldsymbol{\Theta}$*,* $\boldsymbol{\rho}$*, and* $\widehat{\boldsymbol{\Phi}}$*, apply gradient ascent to optimize site locations* $\widehat{\boldsymbol{P}}$*, using the gradient in (20);*
- *Given* $\boldsymbol{V}$*,* $\boldsymbol{\Theta}$*,* $\boldsymbol{\rho}$*, and* $\widehat{\boldsymbol{P}}$*, apply gradient ascent to optimize reference bearings* $\widehat{\boldsymbol{\Phi}}$ *using the partial derivatives in (24).*

TABLE I: System-level parameters for our case study.

Deployment	
P	19 sites that are initially placed on a hexagonal layout with ISD = 500m, three sectors per site, $N = 57$ BSs in total, and $h_{\mathrm{B}} = 25$m.
Existing sites	$\mathcal{S} = \{1, 8, 10, 12, 14, 16, 18\}$, $\widehat{\phi}_i = 30^\circ \quad \forall i \in \mathcal{S}$
Q_{U}	Consisting of $N_U = 4$ aerial corridors
$Q_u, u = 1$	$[-770, -730] \times [-1000, 1000] \times [135, 150]$
$Q_u, u = 2$	$[-1000, 1000] \times [-770, -730] \times [105, 120]$
$Q_u, u = 3$	$[-1000, 1000] \times [730, 770] \times [105, 120]$
$Q_u, u = 4$	$[730, 770] \times [-1000, 1000] \times [135, 150]$
Q_{G}	Square area $[-750, 750] \times [-750, 750]$, $h_{\mathrm{G}} = 1.5$ m
$\lambda_{\mathrm{U}}(\boldsymbol{q})$	Uniform distribution over Q_{U}
$\lambda_{\mathrm{G}}(\boldsymbol{q})$	Gaussian mixture over Q_{G}: $\sum_{i=1}^{4} \pi_i \mathcal{N}(\boldsymbol{\mu}_i, \boldsymbol{\Sigma}_i)$ $\pi_1 = 0.35$, $\boldsymbol{\mu}_1 = [-375, -225]$, $\boldsymbol{\Sigma}_1 = 5 \times 10^4 \boldsymbol{I}$ $\pi_2 = 0.25$, $\boldsymbol{\mu}_2 = [150, 375]$, $\boldsymbol{\Sigma}_2 = 4.2 \times 10^4 \boldsymbol{I}$ $\pi_3 = 0.25$, $\boldsymbol{\mu}_3 = [375, -375]$, $\boldsymbol{\Sigma}_3 = 3.2 \times 10^4 \boldsymbol{I}$ $\pi_4 = 0.15$, $\boldsymbol{\mu}_4 = [-300, 300]$, $\boldsymbol{\Sigma}_4 = 3.8 \times 10^4 \boldsymbol{I}$
$\lambda(\boldsymbol{q})$	$r\lambda_{\mathrm{G}}(\boldsymbol{q}) + (1 - r)\lambda_{\mathrm{U}}(\boldsymbol{q})$, with $r = 0.5$ or $r = 1$
Channel	
$A_{\max}$ and $\rho_{\max}$	14 dBi and 43 dBm, respectively.
$\theta_{3\mathrm{dB}}$ and $\phi_{3\mathrm{dB}}$	10° and 65°, respectively.
$a_{\boldsymbol{q}}$	$\boldsymbol{q} \in Q_{\mathrm{U}}$: 34.02 dB (UMa-AV LoS at 2 GHz, [7])
	$\boldsymbol{q} \in Q_{\mathrm{G}}$: 38.42 dB (UMa NLoS at 2 GHz, [8])
$b_{\boldsymbol{q}}$	$\boldsymbol{q} \in Q_{\mathrm{U}}$: 22 (UMa-AV LoS, [7])
	$\boldsymbol{q} \in Q_{\mathrm{G}}$: 30 (UMa NLoS, [8])

Proposition 6. *Algorithm 1 is an iterative improvement algorithm and it converges.*

Proof. The proof of Proposition 6 is similar to that of other Lloyd-like algorithms [20] and is omitted because of page-limit.

IV. Case Study

In this section, we evaluate the efficacy of our mathematical framework by applying Algorithm 1 on a practical case study.

A. System-level Parameters

Cellular Layout: Simulations are carried out for a practical cellular network comprised of 19 sites, each including three BSs, as modeled in (1) and (2). A total of $N = 57$ BSs are initially positioned on a hexagonal layout with inter-site distance (ISD) of 500 m and the reference horizontal bearing of $\widehat{\phi}_m = 30^\circ$ for each site index m. We assume that all sites $m \in \mathcal{S} = \{1, 8, 10, 12, 14, 16, 18\}$ are fixed a priori as part of the existing infrastructure, while sites $m \notin \mathcal{S}$ are the sites of additional BSs to be deployed.

Channel Model: BSs are equipped with directional antennas with vertical and horizontal half-power beamwidth of $\theta_{3\mathrm{dB}} = 10^\circ$ and $\phi_{3\mathrm{dB}} = 65^\circ$, respectively, and the maximum boresight antenna gain of $A_{\max} = 14$ dBi. The parameters $a_{\boldsymbol{q}}$ and $b_{\boldsymbol{q}}$ are set according to the 3GPP specifications [7], [8] for a carrier frequency of 2 GHz. Without loss of generality, GUEs and UAVs are assumed to be in NLoS and LoS conditions with their serving cell, respectively. All system-level parameters are summarized in Table I.

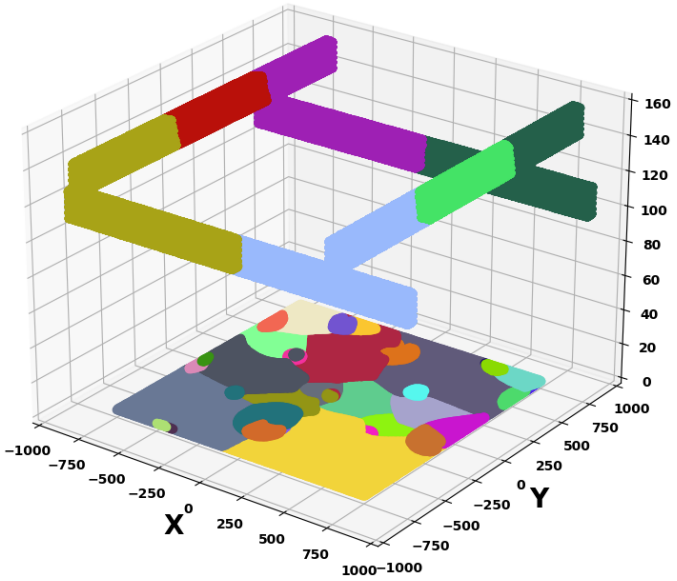

(a) Optimal cell partitioning for GUEs and UAV corridors.

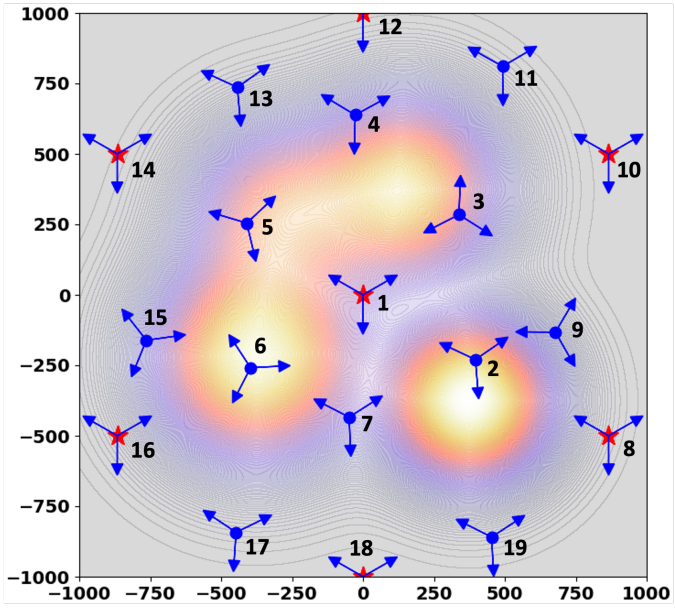

(b) BS locations and orientations overlaid on the GUEs non-homogeneous density. Arrows denote the bearing of each sector.

Fig. 2: Optimal (a) cell partitioning and (b) BS deployment.

B. Coverage-Capacity Optimization for GUEs and UAVs

For the network configuration described in Section IV-A, we run Algorithm 1—with parameters β, κ, and T set to 0.5, 1.0, and -5, respectively—to maximize capacity and coverage as formulated in (12).

Resulting Deployment Configuration: The resulting cell partitioning for GUEs and 3D UAV corridors is depicted in Fig. 2a while the location and orientation of all BSs overlaid on a heatmap of the GUE density are shown in Fig. 2b. Sites marked with red stars in Fig. 2b have fixed locations and reference bearings while the blue circles represent sites that

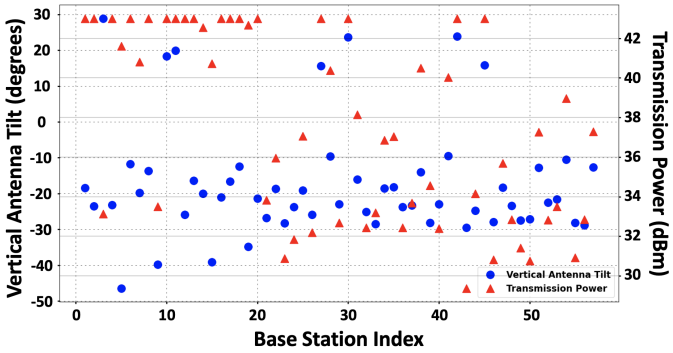

Fig. 3: Optimal BS antenna tilts (blue circles) and transmit powers (red triangles) for $r = 0.5$.

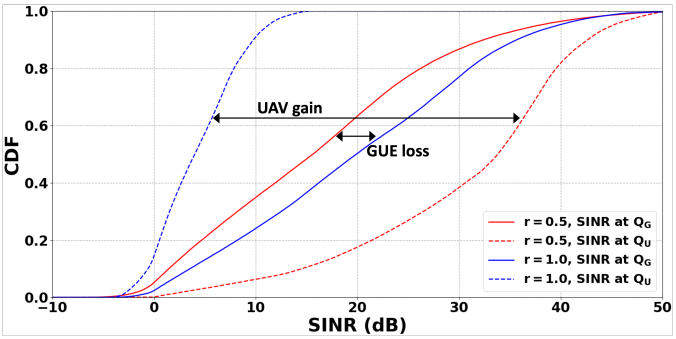

Fig. 4: CDF of the SINR for GUEs (solid) and UAVs (dashed) when the cellular network is optimized for GUEs only ($r = 1.0$) or both ($r = 0.5$).

are optimally positioned and aligned using Algorithm 1. The resulting vertical antenna tilts and transmission powers of all BSs are depicted in Fig. 3. As expected, while the majority of BSs are downtilted (negative tilt angels), some are uptilted to cover the UAV corridors. Moreover, some BSs see their transmit power reduced in order to mitigate interference.

Resulting Performance: In Fig. 4, we plot the CDF of SINR for both GUEs and UAVs. As shown, our joint optimization framework ($r = 0.5$) achieves a substantial improvement in UAV performance (the gap between the dashed blue and dashed red curves) compared to traditional cellular networks, optimized by Algorithm 1 only for GUEs ($r = 1.0$). This gain in UAV performance comes with a relatively minor reduction in the optimal GUE performance (the gap between the solid blue and solid red curves). This demonstrates the effectiveness of our proposed framework in balancing the needs of both user types: it enhances UAV connectivity while minimally impacting the optimal GUE performance, thus achieving a desirable trade-off.

V. Conclusion

We introduced a novel mathematical framework to optimize cellular network deployments for coverage and capacity across a 3D space that accommodates heterogeneous distributions of ground users and UAVs along designated corridors. We derived the necessary conditions and developed an iterative algorithm to fine-tune critical BS parameters—such as location, horizontal bearing, vertical antenna tilt, and transmit power. Our case study demonstrated that the proposed framework significantly enhances UAV connectivity while maintaining near-optimal performance for ground users.

References

[1] G. Geraci *et al.*, "What will the future of UAV cellular communications be? A flight from 5G to 6G," *IEEE Commun. Surveys Tuts.*, vol. 24, no. 3, pp. 1304–1335, 2022.

[2] M. Mozaffari *et al.*, "Toward 6G with connected sky: UAVs and beyond," *IEEE Commun. Mag.*, vol. 59, no. 12, pp. 74–80, 2021.

[3] Q. Wu *et al.*, "A comprehensive overview on 5G-and-beyond networks with UAVs: From communications to sensing and intelligence," *IEEE J. Sel. Areas Commun.*, vol. 39, no. 10, pp. 2912–2945, 2021.

[4] N. Cherif *et al.*, "3D aerial highway: The key enabler of the retail industry transformation," *IEEE Commun. Mag.*, vol. 59, no. 9, pp. 65–71, 2021.

[5] M. Bernabè *et al.*, "Massive MIMO for aerial highways: Enhancing cell selection via SSB beams optimization," *IEEE Open J. Commun. Society*, vol. 5, pp. 3975–3996, 2024.

[6] E. Tekgul *et al.*, "Joint uplink–downlink capacity and coverage optimization via site-specific learning of antenna settings," *IEEE Trans. Wireless Commun.*, vol. 23, no. 5, pp. 4032–4048, 2024.

[7] 3GPP Technical Report 36.777, "Study on enhanced LTE support for aerial vehicles (Release 15)," Dec. 2017.

[8] 3GPP Technical Report 38.901, "Study on channel model for frequencies from 0.5 to 100 GHz (Release 16)," Dec. 2019.

[9] G. Geraci *et al.*, "Integrating terrestrial and non-terrestrial networks: 3D opportunities and challenges," *IEEE Commun. Mag.*, pp. 1–7, 2023.

[10] G. Geraci *et al.*, "Understanding UAV cellular communications: From existing networks to massive MIMO," *IEEE Access*, vol. 6, pp. 67 853–67 865, 2018.

[11] C. Diaz-Vilor *et al.*, "Cell-free UAV networks with wireless fronthaul: Analysis and optimization," *IEEE Trans. on Wireless Commun.*, vol. 23, no. 3, pp. 2054–2069, 2024.

[12] A. Giuliani *et al.*, "Spatially consistent air-to-ground channel modeling via generative neural networks," *IEEE Commun. Lett.*, vol. 13, no. 4, pp. 1158–1162, 2024.

[13] W. Xia *et al.*, "Generative neural network channel modeling for millimeter-wave UAV communication," *IEEE Trans. Wireless Commun.*, pp. 1–1, 2022.

[14] M. Bernabè *et al.*, "On the optimization of cellular networks for UAV aerial corridor support," in *Proc. IEEE Globecom*, 2022, pp. 2969–2974.

[15] S. J. Maeng *et al.*, "Base station antenna uptilt optimization for cellular-connected drone corridors," *IEEE Trans. on Aerospace and Electronic Systems*, 2023.

[16] M. M. U. Chowdhury *et al.*, "Ensuring reliable connectivity to cellular-connected UAVs with up-tilted antennas and interference coordination," *ITU J. Future and Evolving Technol. (arXiv:2108.05090)*, 2021.

[17] S. Singh *et al.*, "Placement of mmWave base stations for serving urban drone corridors," in *Proc. IEEE 93rd VTC*, 2021, pp. 1–6.

[18] C. Diaz-Vilor *et al.*, "Multi-UAV reinforcement learning for data collection in cellular MIMO networks," *IEEE Trans. Wireless Commun.*, vol. 23, no. 10, pp. 15 462–15 476, 2024.

[19] M. Benzaghta *et al.*, "Designing cellular networks for UAV corridors via Bayesian optimization," in *Proc. IEEE Globecom*, 2023, pp. 4552–4557.

[20] S. Karimi-Bidhendi *et al.*, "Optimizing cellular networks for UAV corridors via quantization theory," *IEEE Trans. Wireless Commun.*, pp. 1–1, 2024.

[21] R. M. Gray and D. L. Neuhoff, "Quantization," *IEEE Trans. Inf. Theory*, vol. 44, no. 6, pp. 2325–2383, 1998.

[22] S. Lloyd, "Least squares quantization in PCM," *IEEE Trans. Inf. Theory*, vol. 28, no. 2, pp. 129–137, 1982.

[23] J. Guo and H. Jafarkhani, "Sensor deployment with limited communication range in homogeneous and heterogeneous wireless sensor networks," *IEEE Trans. Wireless Commun.*, vol. 15, no. 10, pp. 6771–6784, 2016.